JOURNAL OF GEOPHYSICAL RESEARCH, VOL. 105, NO. D3, PAGES 3583-3593, FEBRUARY 16, 2000

Behavior of NO_2 and O_3 columns during the eclipse of February 26, 1998, as measured by visible spectroscopy

M. Gil, O. Puentedura and M. Yela
Laboratorio de Atmósfera, Instituto Nacional de Técnica Aeroespacial, Madrid

E. Cuevas
Observatorio de Izaña, Instituto Nacional de Meteorología, Santa Cruz de Tenerife, Spain

Abstract. Observations of the NO_2 and O_3 columns using zenith-viewing differential absorption spectroscopy in the visible range (450-540 nm) were carried out at Izaña Observatory (Tenerife, 28°N, 16°W, 2370 m above sea level.) during the eclipse of February 26, 1998 (95% occultation over the station). Ozone has been retrieved using two different spectral ranges to minimize the effect of the continuous change of the solar spectrum shape as the Sun is being occulted. Small variations before the maximum phase in agreement with previous observations are found, but because of the change in the shape of the solar spectrum, it cannot conclusively be determined whether the ozone changes are real or due to interferences with changing Fraunhofer lines. The difficulties in observing small changes of absorbing gases during solar eclipse when using remote sensing technique that uses the solar UV and visible radiation as the source are discussed. NO_2 displays an increase in phase with the degree of solar occultation, as compared to a non eclipse day of 1.55 ± 0.09. A simple model assuming that changes over short times scales are only due to changes in photodissociation, using O_3 and temperatures obtained from an ozone sounding station close to the observatory, reproduces the observed variation when the NO_2 bulk is assumed to be at an altitude of 28 km. Correction for differences between local solar zenith angle (SZA) and the SZA where the absorption takes place is taken into account.

1. Introduction

Solar eclipses provide rare opportunities to observe the short-term evolution of species of atmospheric interest under photochemical changes. Unlike twilight, when the Earth shadow moves from the surface upward, during eclipses the reduction of the intensity of the light occurs simultaneously at all levels of the atmosphere.

The ratio NO/NO_2 depends critically on the available radiation; consequently, significant changes in the partition of these species are expected to occur during eclipses. A few NO_2 observations have been reported in the literature. *Pommereau et al.* [1976] first measured increases in the column close to the eclipse maximum using a spectrophotometric technique. *Elansky and Elokhov* [1993] reported increases in NO_2 ranging from 55 to 60% during two eclipses, using direct sun measurements at four wavelengths for the first eclipse in 1981 and zenith-scattered light measurements in the 430-450 nm region for the second eclipse in 1990. The same authors estimated a theoretical increase of 1.84 based on a photochemical model by *Gruznev and Elansky* [1982]. *Wuebbles and Chang* [1979] computed the response of a noon eclipse at midlatitudes for a number of stratospheric species at three altitudes (20, 30, and 40 km) using a one-dimensional photochemical model. They calculated increases in NO_2 varying from 1.4 at 20 km to 6.0 at 40 km but concluded in their paper that measurement campaigns were necessary to test the models.

Paper number 1999JD900973.
0148-0227/00/1999JD900973$09.00

The amount of NO_2 in the stratosphere in a non-volcanic situation, as was the case in February 1998 [*Jäger et al.*, 1995], is in photochemical equilibrium during the daytime due to photolysis and the following gas phase reactions:

$$NO_2 + h\nu \rightarrow NO + O(^3P) \quad J_\infty = 1.1 \times 10^{-2}\ s^{-1} \tag{1}$$

$$NO + O_3 \rightarrow NO_2 + O_2 \quad k_2 = 2 \times 10^{-12} \exp(-1400/T) \tag{2}$$

$$O + O_2 + M \rightarrow O_3 + M \quad k_3 = 1.5 \times 10^{-35}[M] \tag{3}$$

The time constants for NO and NO_2 are of the order of 1 min in the altitude range of 20-40 km where the bulk of the NO_2 resides. While other reactions also play a role in the equilibrium of NO_x, during the timescale of an eclipse, the NO_2 increases mainly as the photolysis rate reduces via equation (2). Eclipses take place on timescales short enough to neglect the slow contribution of the production of NO_2 by NO through reactions with ClO and HO_2 and the destruction reactions by O and O_3 on the NO_2 total column.

For a given altitude z the NO_2 during the eclipse at any solar zenith angle may be computed from equations (1) and (2) using an approximation similar to that used by *Solomon and García* [1983] to calculate night time NO_2 concentrations:

$$\frac{[NO]_{day}}{[NO_2]_{day}} = \frac{J_{\infty,NO_2}}{k_2 T(z)[O_3(z)]}, \tag{4}$$

and since

$$[NO_2]_{eclipse} = [NO]_{day} + [NO_2]_{day}, \tag{5}$$

from equations (4) and (5) we get

$$r(sza)=\frac{[NO_2]_{eclipse}}{[NO_2(z,sza)]_{day}}=1+\frac{J_{NO_2}(z,sza)}{k_2T(z)[O_3(z)]}. \quad (6)$$

The evolution of r with the SZA can be computed for every altitude if T, O_3 and J_{NO2} are known.

The column at any SZA then should be

$$[NO_2]_{sza}=\int_0^{top}\frac{[NO_2(z)]_{eclipse}}{r(z,sza)}dz, \quad (7)$$

Where "top" equals the top of the atmosphere. Ground-based zenith measurements provide values of the column at different SZA close to twilight. Assuming that the shape of the NO_2 profile is known, the values during the eclipse can be estimated from equation (6).

J_{NO2} is almost altitude independent in the stratosphere at noon since the visible optical density is low. At low Sun, J_{NO2} is more dependent in altitude and dependent on SZA. During eclipse, J_{NO2} becomes also dependent on the degree of occultation. Assuming the intensity reduction is proportional to the area of solar occultation, this computation can readily be done. From the ratio between NO_2 in a normal day and during the eclipse, the increase due to the eclipse can be calculated. This approximation is valid between 10 and about 38 km where most of the NO_2 column resides. The contribution of lower levels is negligible at very high solar zenith angles when the February 26, 1998, eclipse took place. The higher levels may contribute up to 3.0 % of the column in the subtropical regions.

On the other hand, observations of total ozone during eclipses have been a subject of interest since the pioneering works of *Kawabata* [1937], *Jerlow et al.* [1954], and others. However, there is disagreement among different observations, and still at present this matter is not resolved. *Mims and Mims* [1993] found short-scale fluctuations in the columns after the third contact and almost a 10% reduction near totality, as compared to before the eclipse, using a fast response MicroTOPS spectrophotometer operating at two 5 nm full width at half maximum (FWHM) bands centered at 300 and 306 nm. Subsequently, *Chakrabarty et al.* [1997] presented results qualitatively in agreement with an ozone minimum close to the eclipse maximum phase and an ozone maximum just afterward, the difference being close to 20%. In this case a Dobson spectrophotometer (number 112) operating at wavelength pairs A (305.5 and 325.4 nm) and D (317.6 and 339.8 nm) was used. Previous observations show even more discrepancies. Some authors observe first a slight decrease and then a sharp increase of 4% just before a maximum occultation of 87.5% [*Bojkov*, 1968]. Others show a continuous decrease of some 17% [*Khrgian et al.*, 1965] or no change at all [*Chatterjee et al.*, 1982]. *Osherovich et al.* [1974], using a two-pair wavelength photometer with interference filters 3 nm wide and a telescope driven by a sun tracker, found a decrease between 5 and 11% before and after the maximum, respectively, as compared with before and after the eclipse, and an increase at totality of about 10%. Previously, *Stranz* [1961] found an increase of 4% close to the maximum for a 80% eclipse. *Hunt* [1965] computed theoretically that only a small increase of 1.6 Dobson Units (DU) would occur in the total ozone just after totality assuming a Chapman atmosphere and even less if hydrogen species were included in the scheme, with all changes occurring at altitudes above 50 km because of changes in O_2 photodissociation.

The reason why ozone changes of the reported magnitude should be observed during an eclipse is not clear. Ozone is a long-lived tracer at the levels where the bulk resides and at higher altitudes. Photochemical changes would have an observable effect only in the mesosphere and perhaps the upper stratosphere. At subtropical latitude, the residual ozone column above 40 km is 10 DU (about 3%) and above 50 km is only 1 DU. *Fritts and Luo* [1993] have studied perturbations induced by atmospheric cooling during a solar eclipse caused by the cessation of ozone UV absorption, and they have concluded that pressure changes occur in the form of gravity waves, but the effect would not be significant well into the thermosphere where the amount of ozone is negligible.

All previous ozone observations were performed using spectrophotometers or filter instruments that make direct sun differential absorption measurements by comparing the differential absorption at two wavelengths in the ultraviolet, one with a higher absorption cross section than the other. Generally, a third line (or pair of lines) is used for aerosol correction. The old Russian network M-83 instruments used filters of 40 nm width while newer (after 1969) M-83s and modern M-124s use 15-21 nm half width filters with maximum spectral response at 299 and 325 nm, respectively [*Gushchin et al.*, 1985; *Bojkov et al.*, 1994]. MicroTOPS uses filters of 5 nm FWHM at 300 and 306 nm, and the Dobson spectrophotometer has an average resolution of 1 nm FWHM [*Komhyr*, 1980]. In most of the works the changes in the ratio due to intensity changes at both wavelengths that occur during an eclipse because of the occultation of solar areas of different surface temperatures (limb darkening), which induce the impression of an ozone increase, were corrected on the basis of in the work of *Svensson* [1957]. This author used a correction of the solar intensity at each wavelength by solving the radiative transfer equation for the photosphere under a number of theoretical assumptions as a function of the distance to the center of the solar disk.

It is well known, however [*Phillips*, 1992], that changes in the solar spectrum intensity do not only occur in the continuum from changes in the effective temperature of the Sun surface but are also due to differences in the structure of the chromosphere relative to that of the photosphere. In fact, as the Sun is being occulted, the relative contribution of the chromosphere increases compared with that of the photosphere. In the chromosphere, strong emissions of Balmer lines up to n=34 have been measured, forming a continuum below about 365 nm and decreasing the depth of the Fraunhofer lines of hydrogen. Other elements such as Fe I and Mg I, II and III also contribute saturated lines to the solar absorption. The radiation of the Sun emerges from an altitude that is dependent on the distance to the center of the solar disk, which in turn affects the spectral intensity distribution. In addition, this spatial distribution is far from isotropic. The consequence is that the shape of the solar spectrum is expected to change as the relative contribution by the absorption of the solar elements changes as the occultation proceeds. *Pierce and Slaughter* [1977] computed the solar limb darkening between 303 and 730 nm in 63 discrete wavelengths from observations at the Kitt Peak National Observatory using a high-resolution double monochromator. They provided results on every measured case as constants of a fifth order polynomial fit versus the distance to the center of the solar disk. The tabulated data of Pierce and Slaughter have been used to compute the limb darkening. In Figure 1 a some selected wavelengths are shown normalized to 1 at the disk center, and in figure 1b the ratios between the intensity at the center to that of the limb (and also to a distance radius/2) are shown. In figure 1b, the standard deviation of the polynomial fit is smaller than the symbols used, and the error bars are observed. The results show the nonlinearity of the limb darkening versus wavelength. Even more important, the shape of the function is changing with the distance to the center of the disk. Even though the samples are

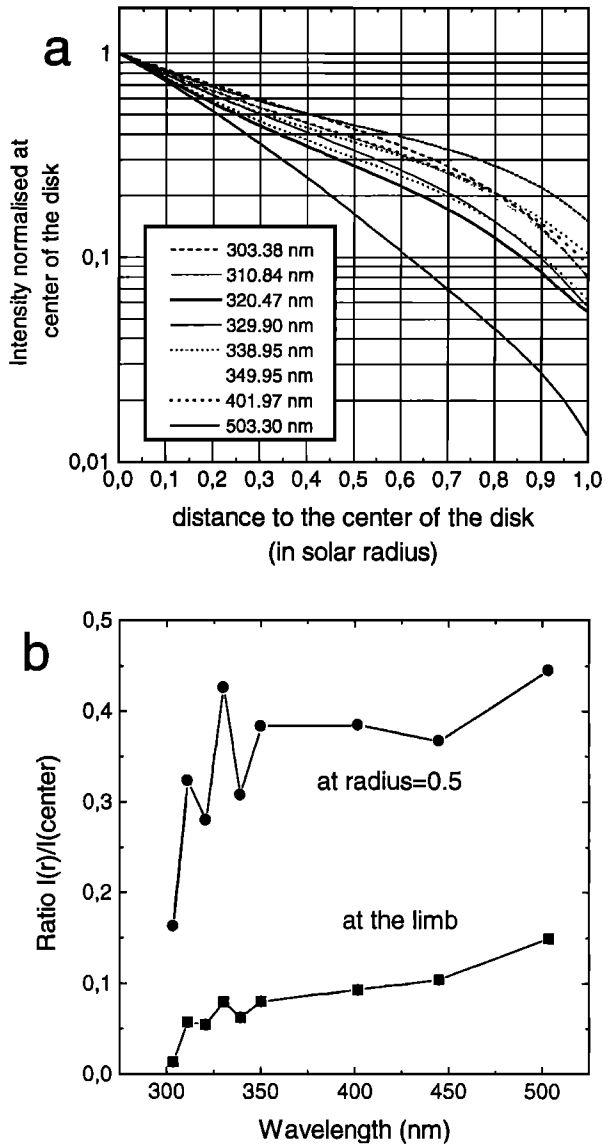

Figure 1. (a) Normalized intensity of the solar disk versus the solar radius for a selected number of wavelengths. (b) The wavelength dependence of the ratio between the center and the limb (solid squares) and the center and a radius of 0.5 (solid circles).

unequally separated between 3 and 20 nm, depending on the range, these data show that great care must be taken when correcting photometer and spectrophotometer measurements for limb darkening effects in observations during a solar eclipse. Moreover, the solar intensity is strongly reduced close to the maximum phase, which increases the noise in the photomultiplier and therefore the overall error.

To overcome the limitation of instruments using two single spectral lines (strictly speaking narrow, bands of a few nanometers), a UV-Vis spectrograph recording the solar spectrum between 340 and 600 nm with a resolution of 1.25 nm FWHM and a sampling of 0.25 nm was deployed at the high-altitude station of Izaña (28°N, 16°W, 2370 m above the sea level). The observations were carried out in zenith sky geometry with the standard procedure used commonly for NO_2 and O_3 measurements. The instrument was set to perform four measurements per SZA degree unless the intensity of the zenith was lower than the minimum accepted, in which case the integration time was automatically adjusted to the maximum signal. The details of the instrument have been previously reported [*Gil et al.*, 1996]. It makes use of a 1024 photo diode array (PDA) detector operating at -40°C to reduce the dark current to low levels. The spectrograph is located inside an isolated hermetic container filled with dry nitrogen and thermally regulated to ±0.5°. The instrument started operation 15 days in advance to provide a stabilization in terms of spectrum shift to less than 0.02 nm/d. The spectral range covered extends from 340 to 600 nm so that selected smaller ranges can be used to retrieve either O_3 or NO_2. For the latter, the standard range of 430-470 nm has been used with the *Coquart et al.* [1995] cross sections at 220 K. Ozone has been retrieved in three different ranges to estimate the interference effects due to changes in the shape of the solar spectrum, using the Global Ozone Monitoring Experiment (GOME) cross sections at 297 K [*Burrows et al.*, 1999]. While the data at laboratory temperature may be unrealistic for the stratosphere, they have been used because a better fit is obtained. Since only relative variations will be considered, changes in the absolute magnitude of the cross sections have no effect on the results.

The instrument employs the differential optical absorption spectroscopy (DOAS) technique. The density of the molecules (N) are obtained by solving the Lambert-Beer equation: $\log(I/I_0) + \Sigma(\sigma N) + f = 0$, providing that the cross sections (σ) are known. Coefficient f accounts for instrumental effects. I_0 is the spectrum measured with the Sun high in the sky, and I is the measurement spectrum close to twilight. By ratioing I/I_0, the strong Fraunhofer structures of the solar spectrum, which are assumed to be constant in time, are eliminated. The differential absorption technique applied to zenith sky observations yields a so-called slant column, which is the weighted average of the column densities seen by an infinite number of rays, scattered at different altitudes at the zenith of the observer, following angled paths from the top of the atmosphere to the zenith of the instrument and vertical paths from the scattering altitude to the instrument [*Noxon et al.*, 1979; *Solomon et al.*, 1987]. A radiative transfer model is used to determine the air mass factors (AMF), which are defined as the coefficient (wavelength and SZA dependent) used to convert the measured columns to the standard "vertical

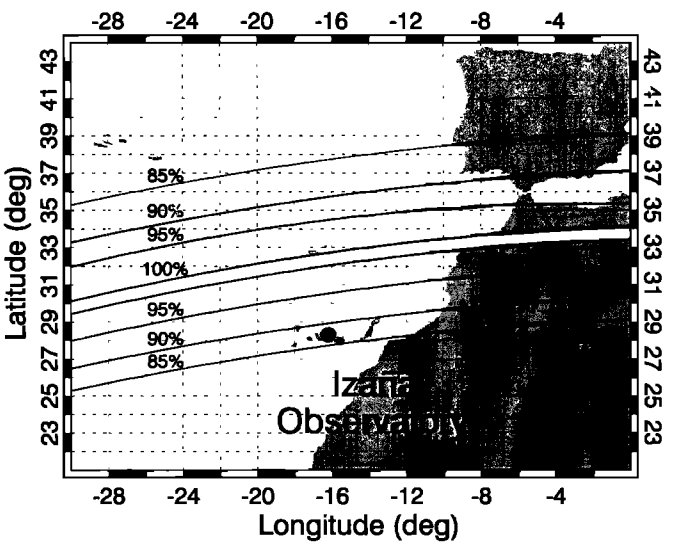

Figure 2. Path of the total eclipse of February 26, 1998, over the Atlantic Ocean showing the magnitudes of maximum occultation. Over Izaña Observatory the maximum of 95% took place at a solar depression angle of 2°.

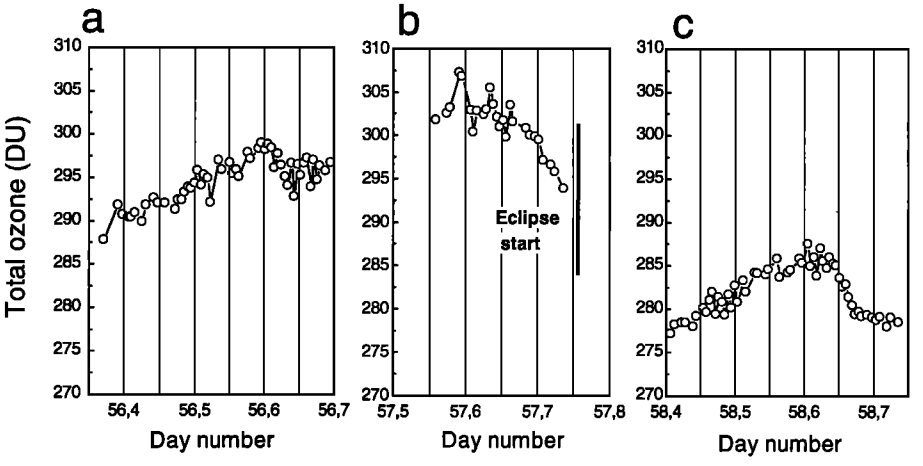

Figure 3. Total ozone as measured by the Brewer MARK-II number 33 instrument at the Izaña Observatory for the days contiguous to the eclipse: (a) February 25, (b) February 26, and (c) February 27. The first contact took place just after the last measurement.

column". The amount contained in the reference spectrum can be estimated by extrapolating to "zero mass" (Langley plot) or by iterative interpolation between morning and evening data and is added to the measured slant column. This technique provides better results during the twilight period when the stratospheric paths are enhanced. We have not found in the literature observations of ozone during an eclipse using visible region spectrometers with new generation diode array detectors that are able to scan simultaneously ranges of tens to hundreds of nanometers.

In this paper we present also data from the day after the eclipse as a means of comparison. O_3 data are compared to the morning of the same day while NO_2 data are compared to the dusk of the next day to avoid the diurnal differences as result from the photodissociation of the N_2O_5 reservoir [*Webster et al.*, 1990]. A single reference spectrum recorded on the morning of February 27 at a SZA of 45° was used for the evaluation of all the measurements in the days contiguous to the eclipse.

2. Eclipse Data and Meteorological Information

The belt of totality of the solar eclipse of February 26, 1998, crossed the Atlantic subtropics some 200 km northward of the Canary Islands (Figure 2). Over the Izaña Observatory the eclipse started in the evening at a SZA of 80° and reached the maximum occultation of 95% with the Sun below the horizon at a SZA of 92° (solar depression angle of 2°). The time between the first contact and the maximum was 56 min. Although measurements were continued up to a SZA of 100°, the intensity dropped strongly, so that reliable results for NO_2 were obtained only up to a SZA of 96° (94° for O_3). Therefore only the first part of the eclipse, just after the maximum occultation, could be observed. At these SZA values the airmass factor enhancement of the O_3 and NO_2 columns is close to maximum.

The meteorological situation in the afternoon of the eclipse was stable with scattered cirrus clouds around the zenith. Eastward winds transporting Saharan dust prevailed during the day of the eclipse. The situation changed during the evening, and on the next day the sky was clear and clean. The filter photometer facility at the Izaña Observatory was used to estimate the optical density at 500 nm as an index of the degree of turbidity. The moderate dust layer had its top 700 m above the station as inferred from the temperature data of the radio sounding of Santa Cruz de Tenerife, only 40 km away from Izaña. The dust is located between two inversion layers. The lower one is at the mixing top at about 800 m and the upper one is at 3000 m. The trajectories computed by the high resolution limited area model (HIRLAM) at the Instituto Nacional de Meteorología (INM) confirm that the Saharan wind was constrained to these levels. Therefore, the extra scattering induced by these particles occurs close to the instrument. In these conditions, while the residual errors rise moderately because of to unknown absorptions in the aerosols and to multiple scattering effects, no discernible changes in the retrieved amounts of gases measured at twilight are found, as confirmed by the 5 years of visible spectroscopy data available at the station (*Yela et al.*, 1998).

Short-term changes in O_3 and NO_2 in the troposphere are not expected to make any contribution to the measured total amount.

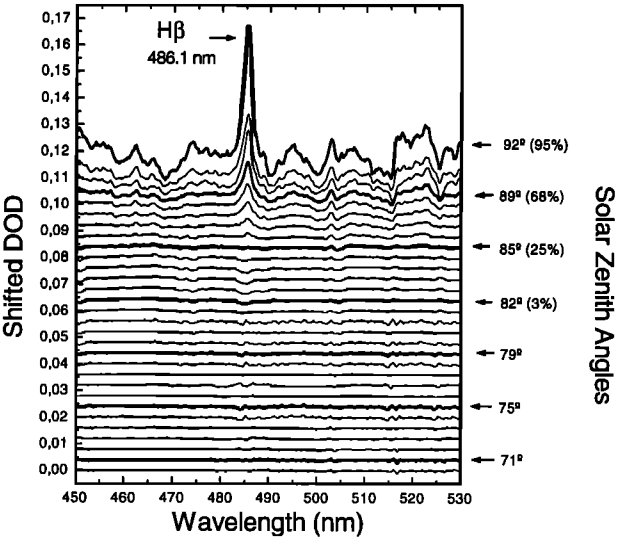

Figure 4. Residuals obtained from the retrieval of ozone for selected spectra at different solar zenith angles before and during the eclipse. A shift of 0.04 Differential Optical Density (DOD) has been applied to each residual spectrum to ease the observation of the curves.

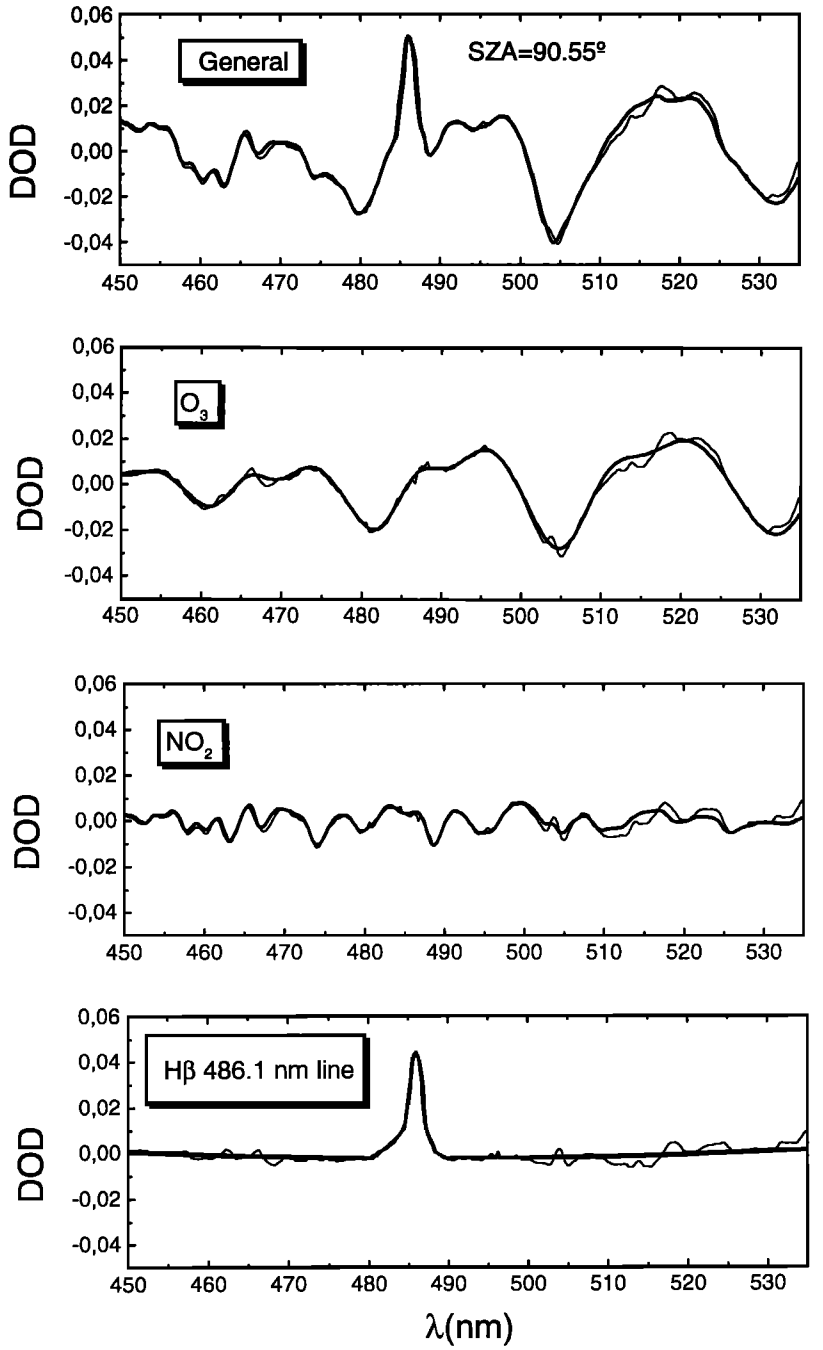

Figure 5. Comparison of the contribution of the absorption of O_3, NO_2, and the Hβ line to the total absorption. The top plot shows the fit obtained including all parameters in the evaluation (O_3, NO_2, H_2O, Rayleigh, O_4, Ring effect, and the Hβ Fraunhofer line).

Surface ozone is routinely measured over the station by the INM with a TECO-49C device. The record for the period of the eclipse shows no change in the decreasing trend during sunset twilight with values of 45 ppbv. On the other hand, NO_2 surface concentrations were measured during the Tropospheric Ozone Research (TOR) Project, yielding values for February well below 40 Parts per trillion (ppt) during the day and below the detection limit of the instrument (15 ppt) at night [*Schultz*, 1995]. These values are representative of a free troposphere in a clean environment, and its contribution to the total column is negligible.

A Brewer spectrophotometer Mark-II operates at Izaña during the high Sun hours. Figure 3 shows the total ozone for the eclipse day and for the previous and subsequent days. Data on eclipse day are more scattered because of the high and variable dust at around noon, which increases the errors. The time of the eclipse start (first contact) is shown in figure 3. Since the eclipse started at a SZA of 80°, no data from the Brewer instrument are available. Total ozone decreased from 300 DU on day 26 to 276 DU on day 27. The rate of dynamic changes over the station is limited to 5 DU/h maximum (1.6 - 1.8% of the column) from the statistic of 1757 cases over a full year. Therefore ozone changes

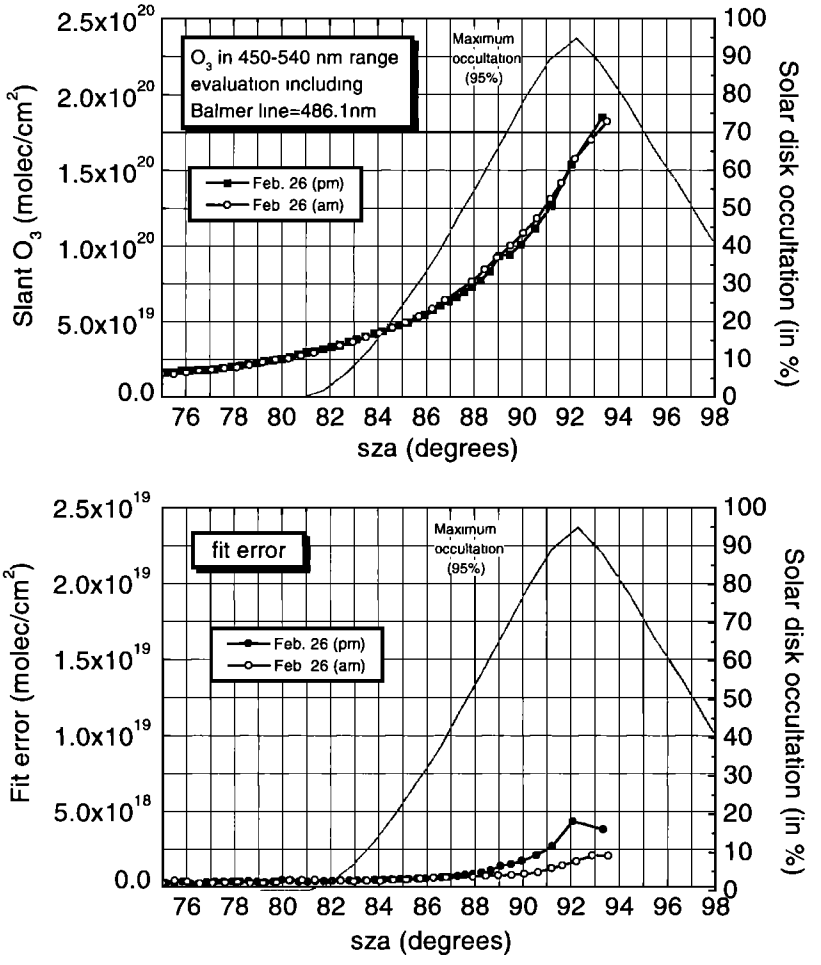

Figure 6. (top) Slant column for ozone in the range 450-540 nm after reevaluation including the Hβ Fraunhofer line. The eclipse data (solid squares) are plotted together with the morning of the same day (open circles). (bottom) Error of the fit. SZA, solar zenith angle.

during the eclipse smaller than this cannot be separated from dynamics.

3. Results and interpretation

3.1. Ozone

Ozone is usually evaluated in the 450-540 nm region where transitions in the Chappuis band occur. Four bands centered at 462, 482, 505, and 532 nm are used for the evaluation. Together with O_3, interfering bands of NO_2, H_2O, and O_4 in this spectral region are included in the fitting procedure. In addition, the contribution of the rotational Raman scattering on air particles (Ring effect) is treated in the evaluation by including pseudo cross sections as the inverse of the twilight spectrum [*McKenzie and Johnston*, 1982]. The results of the ozone slant column during the eclipse yield significantly lower values than those of the same morning, but the measurement errors are up to 1 order of magnitude larger than typical. Since the error increase is in good correlation with the degree of occultation, we suspect that interferences of ozone with hydrogen lines occur. Note that the differential absorption technique assumes that the extraterrestrial spectrum of the Sun has a constant structure.

In order to check the origin of these large errors, we analyzed the structure of the residuals (the differences between the fit and the measurements in terms of differential optical density (DOD)) for the 450-540 nm standard evaluation window, shifted in DOD to facilitate the observation (Figure 4). The residuals dramatically increase as the maximum of the eclipse approaches, and the main contribution of the residual is the Balmer Hβ hydrogen line. These increases mean reduction of absorption in the solar atmosphere when the Sun is partially occulted as compared to the clear full disk.

We have created a line, quasi-Gaussian in shape, of the size and at the position of the Fraunhofer line and have incorporated it in the retrieval analysis as an additional cross section. The relative contribution of each cross section once this correction is applied to the observed DOD is shown in Figure 5. The observed spectrum is shown in thin lines, and the fitted spectrum in thick lines. The top plot is the overall fit, the differential $\log[I/I_0]$, and in the lower panels the individual contributions to the observed absorption are shown. The plotted spectrum was measured at SZA 90.55° when the disk occultation was 85%. The scale is the same for all plots so that the relative contribution of each absorber can be compared. Even though the Hβ line is not positioned in coincidence with the ozone lines, its intensity reaches 4% compared to a noneclipse situation, and its relative contribution is as high as that of ozone. Other changes of lower intensity take place as can be seen by the discrepancy between the observation and the fit.

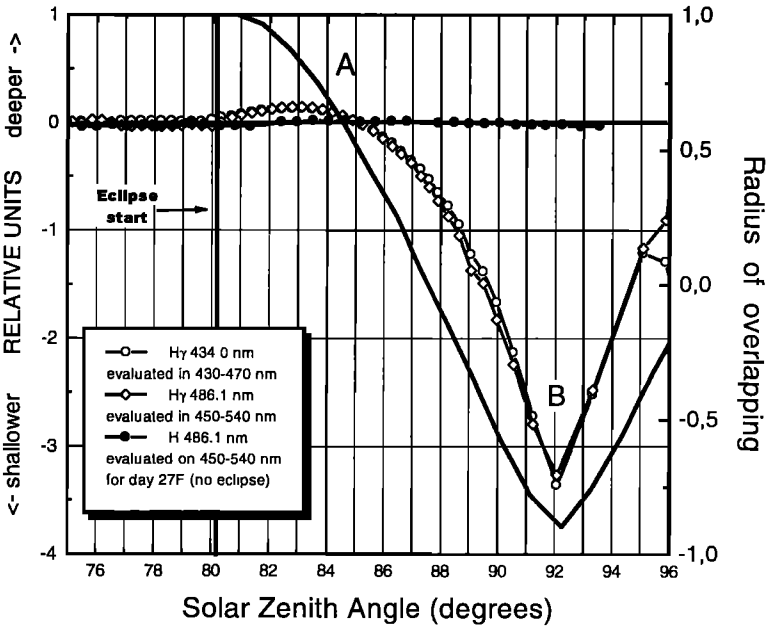

Figure 7. Results of the change of the deepness of the Hydrogen Balmer Fraunhofer lines Hβ 486.1 nm (open diamonds) and Hδ 434.0 nm (open circles) during the eclipse. A and B show the points when the behavior of the hydrogen absorption is inverted (see text). The degree of occultation is plotted in terms of the radius of overlapping thick line, (+1 is the first contact and −1 is the total eclipse). Solid circles show the result of the evaluation for the next day of the eclipse (February 27 evening, Hβ line) to test possible interferences between absorbers.

After the reanalysis the ozone slant column during the eclipse is closer to the morning one, confirming the interference effect previously suspected (Figure 6). We have also examined the data in our standard range for NO_2 retrieval (430-470 nm). Since the Hγ line at 434.0 is present here, the same procedure was applied to the evaluation. The results in this case show almost no effect up to SZA of 90° and a slight increase afterward (not shown). However, although the fit in this range is better, the ozone differential absorption lines at 442 and 461 nm are small resulting in a high absolute error.

The results of the retrieval of the hydrogen lines Hβ and Hγ are shown in Figure 7 to compare the behavior of the changes of solar absorption at different wavelengths during the eclipse. In figure 7, the occultation in units of solar radius of overlapping is shown. Plus one means first contact, and minus one means total eclipse. The scale of this curve is at the right-hand side. Both hydrogen lines show identical behavior. During the first phase, just after the first contact, the lines get slightly deeper as the moon covers part of the solar chromosphere. When the overlap reaches −0.25 of the solar radius (point A in the Figure 7), the effect of the occulted atmosphere compensates the occulted inner part of the Sun. From that point the absorption starts to decrease strongly in phase with the degree of occultation up to the maximum (point B in the Figure 7). We have tested the possible interference of the inclusion of these lines with other absorbers by evaluating a noneclipse day (February 27, evening) using the same procedure. The result shows no change in the intensity of the Hβ line as can be expected if the line does not interfere with other absorbers.

From the observation of the residuals it becomes evident that the hydrogen lines are not the only problem when attempting to measure ozone during a solar eclipse by remote sensing based on ultraviolet and/or visible instruments. Smaller changes in the spectrum occur because of changes in absorption of other elements in the solar atmosphere that cannot be eliminated. To improve the fit, we finally selected a new range where no hydrogen lines are present, at 435-485 nm. The result of this third evaluation using the standard procedure shows little difference with the evaluation in the 430-470 nm range including the Hγ line. In this case, the fit error is larger than that in the previous case, but the overall error is lower because of the higher differential absorption cross section at 482 nm compared to 461 and 442 nm (Figure 8).

The results from the different evaluation windows can be quantitatively compared by obtaining the ratio between morning and evening after normalization at a SZA of 75°-80° (before the eclipse start) to account for possible variability during the day. For this operation we need to assume that the AMF does not change owing to the eclipse. As *Sarkissian et al.* [1995] have exhaustively analyzed, the AMF does change owing to a number of factors, such as the altitude of the layer, the concentration of aerosols, a change in cross sections, the characteristics of the model, the air density, etc. Solar eclipses perturb the middle atmosphere owing to changes in photodissociation rates, cooling by ozone implying changes in density, etc., that could affect the AMF. While the lower mesosphere may have some, even very small, contribution to the AMF [see *Sarkissian et al.*, 1995], the effect of the eclipse on temperature changes should have a negligible influence on the AMF. Expected changes in the temperature are as low as 0.2 K at 40 km [*Herman*, 1979] and less at lower altitudes. On the other hand, the increase in NO_2 during the eclipse could also modify the standard AMF values used at twilight. However, since the J_{NO2} has very little altitude dependence in the stratosphere, no significant changes in the shape of the profile are expected to occur. To quantify this effect, the single scattering model in use at the Instituto Nacional de Técnica Aeroespacial (INTA) has been run under different stratospheric conditions and for changes in the NO_2 profile. Results show that the differences are smaller than 1%.

The evening to morning ratio of derived vertical column

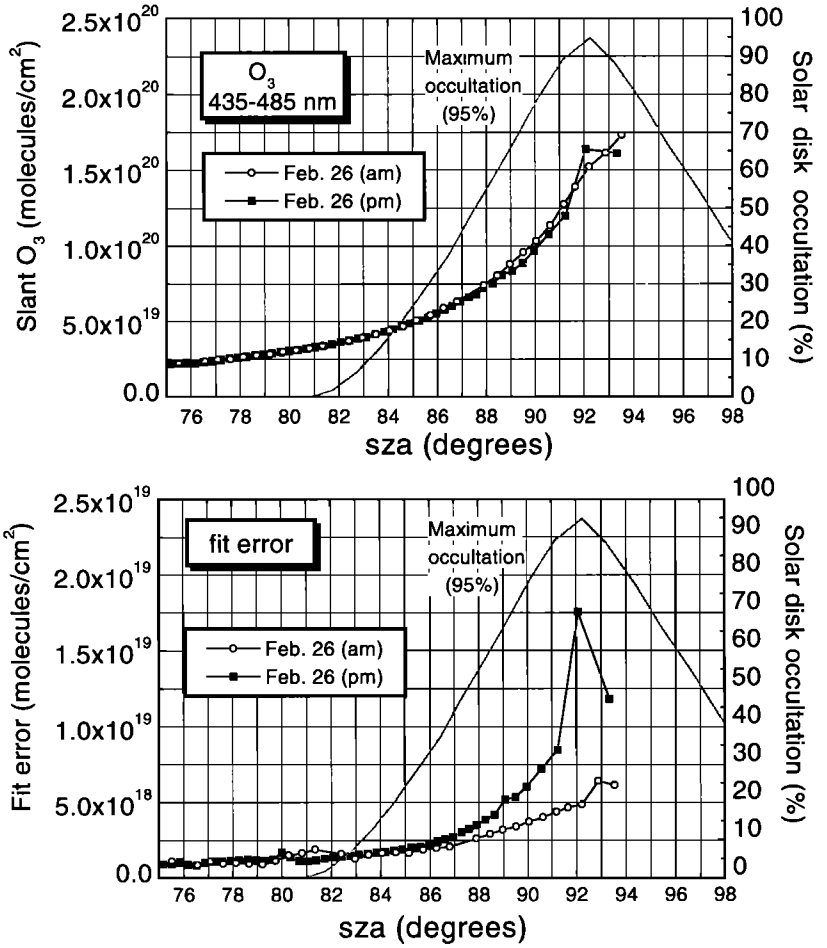

Figure 8. As in Figure 6 but for the range 435-485 nm, out of hydrogen lines' influence.

ozone has been plotted in Figure 9. In Figure 9d the ratio of the day after the eclipse has been plotted as a reference for what can be expected in a noneclipse situation. The error bars in these cases include the error of each ratioed measurement computed by the error propagation theory. The technique at zenith provides better signal at around 90° when the stratospheric absorbers are enhanced and the intensity of available light is high enough for short integration times (<50 s). At lower SZA the absorption is less, and the relative error increases. On the other hand, with very high SZA (>93°), other atmospheric effects (multiple scattering, changes in the structures of cross sections as the altitude scanned is different, etc.) and instrumental effects (longer integration times) have to be taken into account. In Figure 9d the error bars become smaller as the SZA increases, because the absorption enhancement compensates the increase of the residuals. The observed reduction at 88°-90° could be due to real changes in ozone during this period of the day or due to changes in the AMF. Figures 9a and 9b show the ratios of the ozone evaluated in the standard 450-540 and 435-485 nm windows, respectively. An ozone increase is observed just before the maximum after 91° but since in this phase the error was high owing to the previously mentioned changes in the Fraunhofer structures of the solar spectrum, this result must be observed with care. Error bars are smaller in the range 450-540 nm where more O_3 bands are available. The average of the evaluation in the two windows is plotted in Figure 9c. The observations using visible spectroscopy agree well with the results of *Bojkov* [1968] and *Osherovich et al.* [1974], since a smooth decrease can be observed after the beginning of the eclipse of up to 7% and a sharp increase of 4% can be observed just before the maximum of the eclipse. This agreement is remarkable, considering the use of a quite different technique and spectral range, supporting these previous studies. It must be noted, however, that the variations are within observational error bars that are higher than those typical, owing to the difficulties of making remote sensing observations during the eclipse, and cannot conclusively be attributed to real changes in ozone.

3.2. NO_2

Fast changes in the total NO_2 column are expected to occur during a solar eclipse from the reduction of photolysis as the Sun is blocked by the Moon. According to gas phase chemistry, the increases should occur in phase with the degree of the reduction of available light. The amount of increase for a total eclipse was estimated by *Gruznev and Elansky* [1982] to be 84%. In this work we estimated the increase in NO_2 vertical column by comparing the evening's twilight of the eclipse with the next evening's twilight. To account for changes due to transport, we compared the morning data in days adjacent to the eclipse. During these days, the column was decreasing from 2.67×10^{15} to 1.85×10^{15} molecules/cm^2. All spectra have been evaluated with the same reference spectrum; therefore relative comparisons can be made. The results are displayed in Figure 10. Both morning

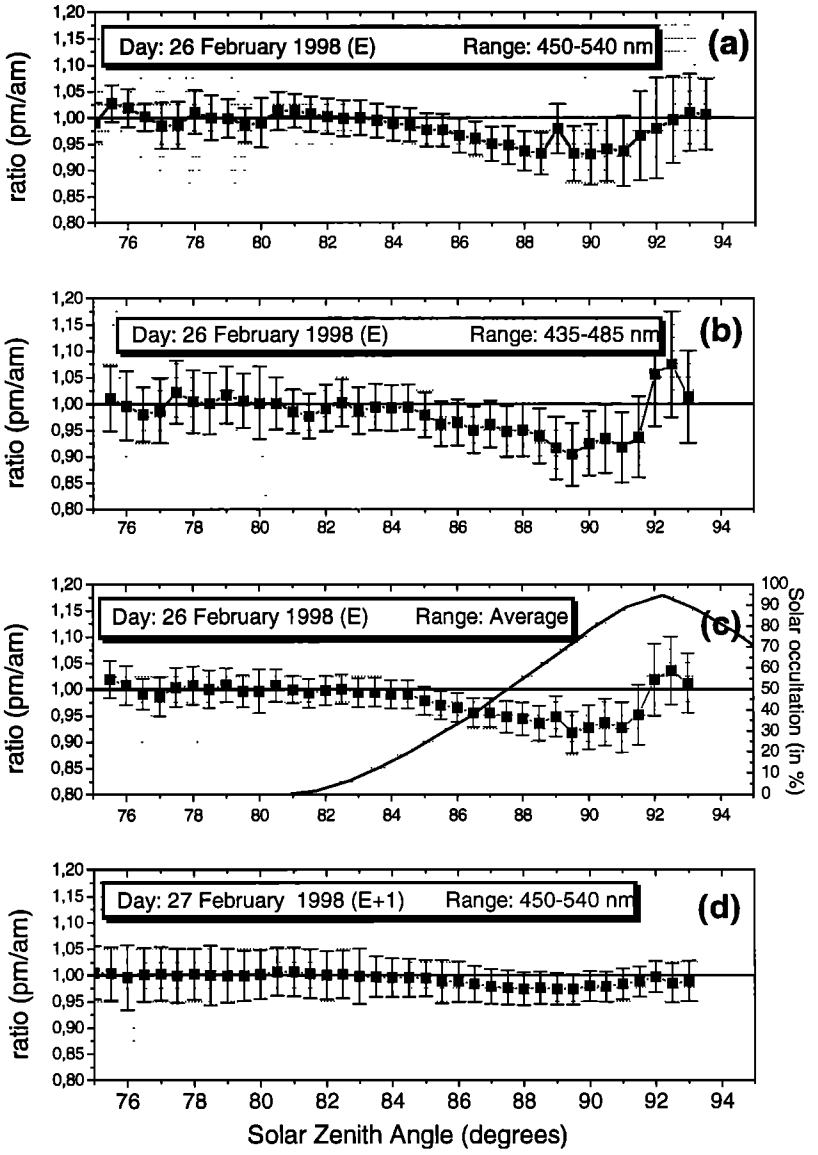

Figure 9. Evening to morning ratio of ozone versus SZA for (a-b) the two retrieved ranges and (c) the average. The solar disk occultation is shown in Figure 9c. (d) The evening to morning ratio for a noneclipse day. Error bars represent the fir erros.

and afternoon data have been normalized using the data between a SZA of 75° and 80°. The data of February 27 have been multiplied by a factor of 1.09 for the morning data set and 1.02 for the afternoon data set. Displaying the morning data shows that no significant changes in the AMF due to atmospheric effects have occurred. The error bars represent the error of the fit, estimated in molecules/cm^2. For clarity, the error bars of the E+1 dusk are not shown, but they are very close to the morning ones. On the other hand, the afternoon data on the eclipse twilight show a very significant increase in fit error as previously seen in the O_3 case. Although some of this increase is caused by the reduction of the available light, most of it is a consequence of the change in the shape of the solar spectrum. However, the increase in the NO_2 column due to the eclipse is significant, as it is much larger than the error bars of the individual measurements.

The quantification of the increase due to the eclipse has been done, as in the case of ozone, by first interpolating so that values are obtained for both data sets at the same SZA and then normalizing the data using the 75°-79° SZA range to correct for variations, not related to the eclipse, on the two successive days. The ratios between both normalized data sets are displayed in Figure 11. In this case the bars are those resulting from error propagation for the two data sets. The increase starts in phase with the disk occultation and reaches its maximum at maximum occultation. A value of 1.55 ± 0.09 has been obtained, in good agreement with the previous observations of *Elansky and Elhokov* [1993], who measured a maximum of 99.7% occultation occurring at 87° in the morning. Rough estimates of the ratio in total column can be extracted from the work of *Wuebbles and Chang* [1979] by fitting the ratios at the given altitudes and applying this function to a standard profile, assuming that the bulk of the NO_2 layer at subtropical latitudes in February is located between 26 and 29 km (Stratospheric Aerosol and Gas Experiment (SAGE) data 1989, available from Greenhouse Effect Detection Experiment [NASA, 1992]. The ratio obtained

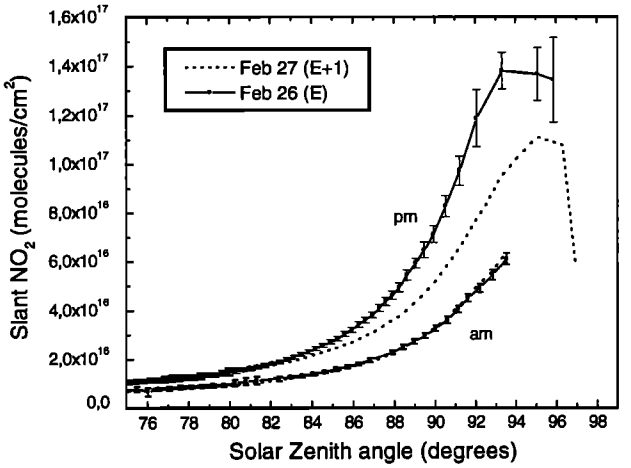

Figure 10. Slant column of NO_2 retrieved in the 430-470 nm range for the day of the eclipse (solid line) and the next day (dashed line).

for the column is 2.4, for an eclipse around noon at 50° latitude in winter. The amount of increase is dependent on the SZA. We expect higher ratios of increase at noon than at twilight since part of the daily NO has already been converted to NO_2 at very large solar zenith angles. We have made calculations from equation (6) using the single scattering AMF model of INTA to compute flux at each altitude and SZA from the surface to 90 km altitude. Profiles of ozone and temperature from an ozonesonde launched close to the station on the day before the eclipse, extrapolated assuming constant mixing ratio above the top of the sounding, were used. An NO_2 profile from the Air Force Geophysics Laboratory (AFGL) database for tropical regions was scaled to the values of the vertical column measured in the ground in the evening (2.75×10^{15} molecules/cm^2).

It is important to note that when using UV-Vis spectroscopy in zenith-viewing geometry, the observations refer to an air mass in the stratosphere that is not vertical but shifted in the direction of the Sun. When the Sun is below the horizon, most of the observed air mass is approximately at the tangent point [Solomon et al., 1987]. We must then consider the local SZA (lsza in the following) and the real SZA at the location of the air mass (rsza). The difference between them in the middle stratosphere when the lsza of the solar occultation was maximum (lsza=92°) is about 2° in longitude, which represents a significant difference in the computation of the ratio of the increase (the latitudinal correction is negligible at this measurement latitude). It is therefore customary to consider both the J computation and the degree of solar occultation in this correction. We can say that the maximum occultation occurred at a rsza of 90° when the NO_2 photodissociation rate is still significant. In Figure 11 the results of the model are shown, assuming most of the layer is at three different altitudes between 26 and 30 km. The model has been validated since it reproduces the increase observed at twilight under a noneclipse situation. The best fit is obtained for a NO_2 average altitude of 28 km. The higher values (during the first phase of the eclipse) compared to the model arise because a constant shift of 2° was applied as a correction factor. This is strictly only valid at 92° lsza, while at 80°-85° lsza, the air mass observed by the instrument is close to the vertical, and so rsza and lsza are almost coincident. The opposite is true for the highest SZA. In this case, the model should have been shifted by more than 2°. In Figure 11 the solar disk occultation has been plotted for the rsza. The increase factor plotted versus the real solar disk occultation yields a correlation coefficient of 0.996.

The results of this simple model have been validated for a single altitude of 30 km using a box model including a full NO_y family based on the Phodis package (A. Killing, Phodis: a program package for calculation of photodissociation rates in the Earth atmosphere, available by anonymous ftp at ftp.itec.norut.no, 1995) for computing the photodissociation rates and the ASAD (A Self-contained Atmospheric chemistry coDe) package for solution of the equation system with the IMPACT solver [*Carver et al.*, 1997]. The reaction rates have been extracted from the report of *Demore et al.* [1994]. The results of both models are within 1%, confirming that the short-scale twilight changes in NO_2 are driven only by the photodissociation rate, J, and the NO_2 production through the reaction of nitrogen monoxide with ozone.

4. Conclusions

O_3 and NO_2 observations show variations in the columns that depend on the degree of occultation. The technique used in this study shows the difficulties of observing small variations of the column due to changes in the structure of the extraterrestrial solar spectrum during an eclipse on scales of a few nanometers. Two spectral windows were considered for O_3 retrieval to reduce the effect of the changing Fraunhofer spectrum, yielding a statistically significant smooth ozone decrease up to 7%, followed by a sharp increase of 4% near the maximum occultation (95%). These data are in good agreement with the direct Sun ultraviolet observation of *Bojkov* [1968] using a Dobson spectrophotometer and also of *Osherovich et al.* [1974] using a dual photometer. However, large error bars in the fit of the data preclude an unequivocal statement that this behavior is real. The fast, small changes in ozone during the eclipse as observed using solar radiation must be confirmed by an alternative technique that does not make use of the Sun as the light source.

On the other hand, the NO_2 column increases rapidly as the eclipse starts. The maximum increase factor of 1.55 ± 0.09 at the local solar zenith angle where the occultation is maximum is in good agreement with previous observations by *Elansky and*

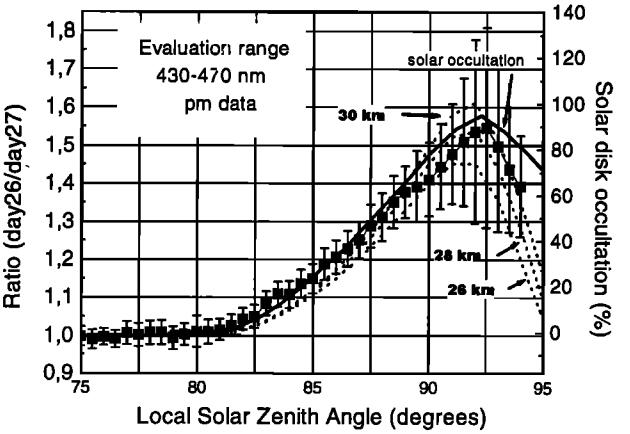

Figure 11. Ratio of NO_2 slant column for February 26, 1998, divided by that for February 27, 1998. Data have been normalized using the data from 75°-80° before the eclipse started. Error bars represent the fit error of the ratio computed by error propagation. The results of the increase in NO_2 as calculated by equation (6) are shown (dashed lines) for different altitudes of the layer. The model computes the J at the ray's tangent point (SZA=90°). The degree of occultation in this case has been represented in terms of the real air mass observed, 2° westward of the station.

Elohkov [1993]. A simple model (based on the formulae of *Solomon and García* [1983] based only on the actual ozone mixing ratio, the NO + O_3 reaction rate at measured temperatures, and J_{NO2}) reproduces the observations when the bulk of the NO_2 is assumed to be at an altitude of 28 km, after correcting for the differences between the local solar zenith angle and the real solar zenith angle at this altitude.

Acknowledgments. We want to thank Xavier Calbet from the INM for the data on occultation during the eclipse over Izaña, all the Izaña GAW station staff for the assistance in the instrument operation and ancillary data support, and Conchita Parrondo for graphical assistance. This work has been possible thanks to the support of the UE through the SCUVS-3 Project (ENV-4-CT95-0089).

References

Bojkov, R., The ozone variations during the solar eclipse of 20 May 1966, *Tellus*, *20*, 417-421, 1968.

Bojkov, R.D., V.E. Fioletov, and A.C. Shalamjansky, Total ozone over Eurasia since 1973 based on reevaluated filter ozonometer data, *J. Geophys. Res.*, *99*(D11), 22,985-22,999, 1994.

Burrows, J. P., A. Richter, A. Dehn, B. Deters, S. Himmelman, S. Voigt, and J. Orphal, Atmospheric remote-sensing reference data from GOME, part 2, Temperature-dependent absorption cross-sections of O_3, *J. Quant. Spectrosc. Radiat. Transfer*, *61*, 509-517, 1999.

Carver, G., P.D. Brown and O. Wild, The ASAD atmospheric chemistry integration package and chemical reaction database, *Comp. Phys. Comm.*, *105*, 197-215, 1997.

Chakrabarty, D.K., N.C. Shah, and K.V. Pandya, Fluctuation in ozone column over Hamedabad during the solar eclipse of 24 October 1995, *Geophys. Res. Lett.*, *24*(23), 3001-3003, 1997.

Chatterjee, K., H. S. Ahuja, and C.K. Chandrasekharan, Total ozone, surface ozone and vertical distribution of atmospheric ozone measurements conducted at Gadag and other stations in India during the total solar eclipse of 16 February 1980, *Proc Indian Acad. Sci, Sect. 48 A*, Suppl. 3, 125-130, 1982.

Coquart, B, A Jenouvrier, and M F. Merienne, The NO_2 absorption spectrum, II, absorption cross sections at low temperature in the 400-500nm region, *J. Atmos. Chem*, *21*, 251-261, 1995.

Demore, W.B., S.P. Sander, D.M. Golden, R.F. Hampson, M.J. Kurylo, C.J. Howard, A.R. Ravishankara, C.E. Kolb, and M J. Molina, Chemical kinetics and photochemical data for use in stratospheric modelling, *JPL Publ.*, *94-26*, 192, 1994.

Elansky, N.F., and A.S. Elokhov, Variation of stratospheric NO_2 during the solar eclipse, in *Ozone in the troposphere and the stratosphere, part 2, NASA Conf. Publ. 3266, Procc. of 1992 Quadrenn. Ozone Symp.* 699-702, 1993.

Fritts, D.C., and Z. Luo, Gravity wave forcing in the middle atmosphere due to reduced ozone heating during a solar eclipse, *J. Geophys. Res.*, *98*(D2), 3011-3021, 1993.

Gil, M., O. Puentedura, M. Yela, C. Parrondo, D.B. Jadhav, and B. Thorkelsson, OClO, NO_2 and O_3 total column observations over Iceland during the winter 1993/94, *Geophys. Res. Lett.*, *23*(23), 3337-3340, 1996.

Gruznev, N.F., and N.F. Elansky, Changes in stratospheric constituents during a solar eclipse, *Izv.Acad. Sci. USSR Atmos. Oceanic Phys., Eng. Trans.*, *18*, 541-544, 1982.

Gushchin, G.P., S.A. Sokolenco, and V.A. Kovalyov, Total ozone measuring instruments used in the USSR station network, in *Atmospheric Ozone*, edited by C.S. Zerefos and A. Ghazi, p.543, D. Reidel, Norwell, Mass., 1985.

Herman, I.R., The response of stratospheric constituents to a solar eclipse, sunrise and sunset, *J. Geophys. Res.*, *84*(C7), 3701-3710, 1979.

Hunt, B.G., A theoretical study to the changes occurring in the ozonosphere during the total eclipse of the Sun, *Tellus*, *17*, *4*, 517-523, 1965.

Jager, H., V. Freudenthaler, and H. Homsburg, Aerosol lidar observations at Garmish-Partenkirchen during SESAME, Polar Stratospheric Ozone 1995, *Air Pollut. Res. Rep. 56*, 154-157, Eur. Comm., Brussels, 1995.

Kawabata, I., Spectrographic observations on the amount of the atmospheric ozone at the total eclipse of June 19, 1936, *Jpn. J. Astron. and Geophys.*, *14*,1-3, 1937.

Khrgian, A. K., G.I. Kuznetsov, and A.V. Kondrat'eva, *Atmospheric Ozone*, edited by D.I. Nasilov, Izdatel'stvo Nauka, Moscow, 1965, English translation, Isr. Program for Sci. Trans., Jerusalem, 1967

Kohmyr, W. D., Operation handbook: Ozone observations with a Dobson spectrophotometer, *WMO-Rep. 6*, World Meteorol. Organ. Global Ozone Res. and Monit. Proj., Geneva, 1980.

McKenzie, R.L., and P.V. Johnston, Seasonal variations in stratospheric NO_2 at 45°SW. *Geophys. Res. Lett*, *9*(2), 1255-1258, 1982.

Mims, F. M., III, and E. R. Mims, Fluctuations in column ozone during the total eclipse of July 11, 1991, *Geophys. Res. Lett.*, *20*(5), 367-370, 1993.

NASA, Greehouse Effect Detection (GEDEX), [CD-ROM], Goddard Space Flight Center, Greenbelt, Md., 1992.

Noxon, J.F., E C. Whipple Jr., and R.S. Hyde, Stratospheric NO_2., 1, Observational method and behavior at mid-latitude, *J. Geophys. Res.*, *84*(8), 5047-5065, 1979.

Osherovich, A.N., N. Shpanov, and V. Zarubaylo, Measurement of total ozone content during the total solar eclipse of 10 July 1972, *Atmos. Ocean Phys.*, *10*, 755-757, 1974.

Phillips, K.J.H., *Guide to the Sun*, Cambridge Univ. Press, New York. 1992.

Pierce, A.K., and C.D. Slaughter, Solar limb darkening, I, (3033-7297Å), *Sol. Phys.*, *51*, 25-41, 1977.

Pommereau, J.-P., A. Hauchecorne, and G. Souchon, Variation of the atmospheric NO_2 total content observed during a solar eclipse: Diurnal variation in the tropics, *C. R. Seances Acad. Sci., Ser. B*, *283*(5), 163-165, 1976.

Sarkissian, A., H.K. Roscoe, and D.J. Fish, Ozone measurements by zenith-sky spectrometers: An evaluation of errors in air-mass factors calculated by radiative transfer models, *J. Quant. Spectrosc. Radiat. Transfer*, *54*(3), 471-480, 1995.

Schultz, M., Die Bedeutung von Stickoxiden fuer die Ozonbilanz in Reinluftgebieten Untersuchung der Photochemie in Reinluft anhand von Spurengasmessungen in Teneriffa, *PhD thesis*, 162 pp, *University of Wuppertal*, , 1995.

Solomon, S., and R García, On the distribution of nitrogen dioxide in the high-latitude stratosphere, *J. Geophys. Res.*, *88*(9), 5229-5239, 1983.

Solomon, S , A.L. Schmeltekopft, and R.W. Sanders, On the interpretation of zenith sky absorption measurements, *J. Geophys. Res.*, *92*(D7), 8311-8319, 1987.

Stranz, D., Ozone measurements during solar eclipse, *Tellus*, *13*, 276-279, 1961.

Svensson, B., Observations on the amount of ozone by Dobson spectrophotometer during the solar eclipse of June 30, 1954, *Ark. Geofys.*, *2*(28), 573-594, 1957.

Webster, C R., R.D. May, R. Toumi, and J.A. Pyle, Active nitrogen partitioning and the nightime formation of N_2O_5 in the Stratosphere: Simultaneous in situ measurements of NO, NO_2, HNO_3, O_3 and N_2O using the BLISS diode laser spectrometer, *J. Geophys. Res.*, *95*(D9), 13,851-13,866, 1990.

Wuebbles, D., and J.S. Chang, A theoretical study of stratospheric trace species variations during a solar eclipse, *Geophys. Res. Lett.*, *6*(3), 179-182, 1979.

Yela, M., M. Gil, M. Navarro, S. Rodriguez, E. Cuevas, and C. Romero, Meridional transport in the subtropics during winter as seen by NO_2 column record, in *Polar Stratospheric Ozone 1997*, edited by N.R.P. Harris, I. Kilbane-Dawe and G.T. Amanatidis, *Air Pollut. Rep. 66*, pp. 88-91, Eur. Comm., Brussels, 1998.

E. Cuevas, Observatorio de Izaña, INM, San Sebastián 77, 38071 Santa Cruz de Tenerife. Spain. (ecuevas@inm.es)

M. Gil, O. Puentedura, and M. Yela, Laboratorio de Atmósfera. INTA. Ctra de Ajalvir km 4, Torrejón de Ardoz, 28850 Madrid., Spain. (gilm@inta.es; puentero@inta.es; yelam@inta.es)

(Received February 4, 1999; revised September 10, 1999; accepted September 13, 1999).